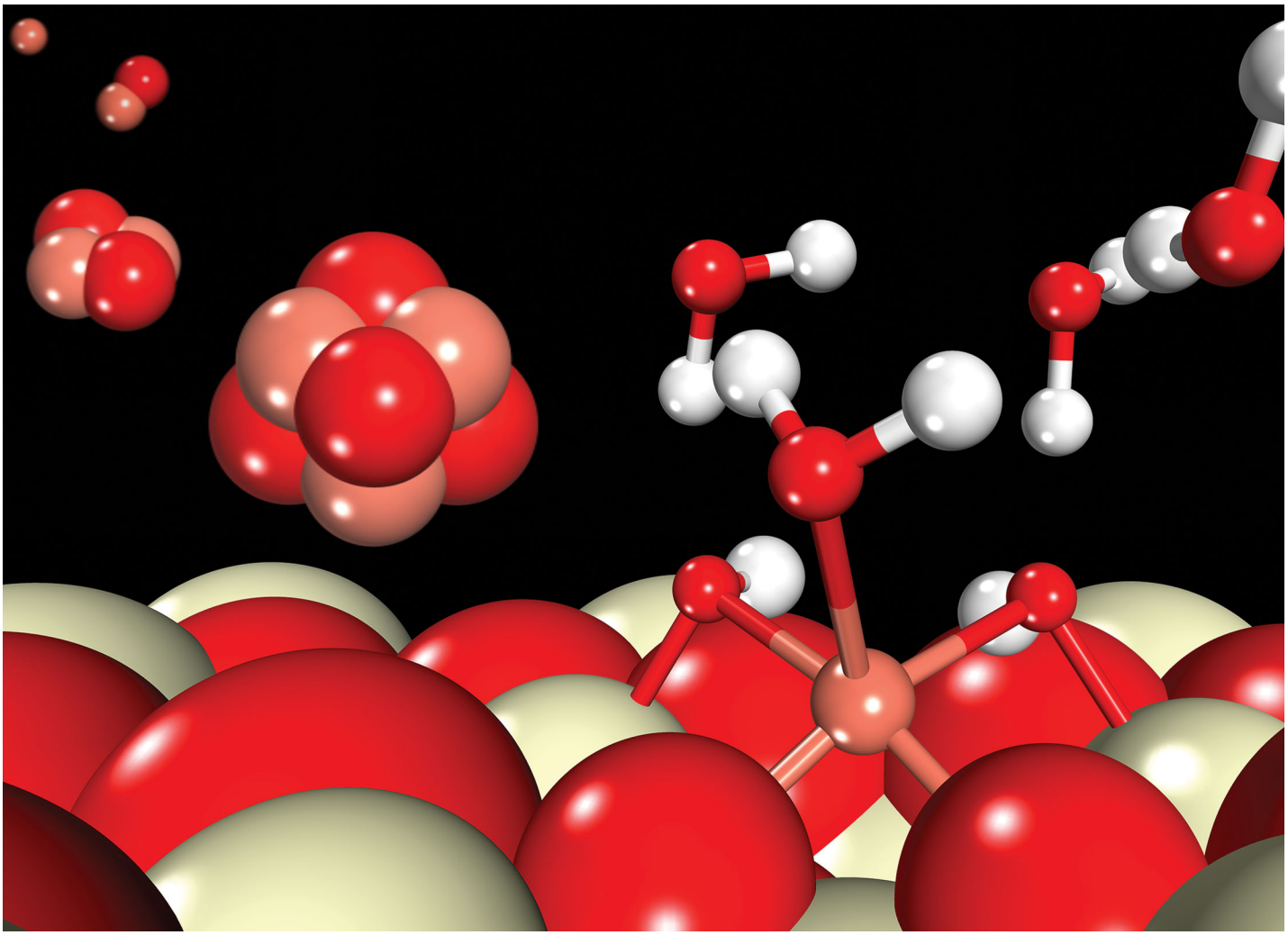

Showcasing research from the group of Prof. C. Richard A. Catlow FRS at the UK Catalysis Hub based at the Rutherford Appleton Laboratory, United Kingdom.

The adsorption of Cu on the CeO_2(110) surface

This work reports a detailed density functional theory (DFT) study in conjunction with extended X-ray absorption fine structure (EXAFS) experiments performed at the UK Catalysis Hub on the geometrical and local electronic properties of various Cu species on the CeO_2(110) surface. We demonstrate the effect of oxidation states and solvent environment on the electronic properties of the adsorbed Cu species for this important class of catalysts.

As featured in:

See Arunabhiram Chutia, C. Richard A. Catlow *et al.*, *Phys. Chem. Chem. Phys.*, 2017, **19**, 27191.

ROYAL SOCIETY OF CHEMISTRY

rsc.li/pccp

Registered charity number: 207890

PCCP

PAPER

View Article Online
View Journal | View Issue

Cite this: *Phys. Chem. Chem. Phys.*, 2017, **19**, 27191

The adsorption of Cu on the CeO_2(110) surface†‡

Arunabhiram Chutia, *[ab] Emma K. Gibson, [ab] Matthew R. Farrow, [b] Peter P. Wells, [acd] David O. Scanlon, [bd] Nikolaos Dimitratos, [e] David J. Willock [e] and C. Richard A. Catlow *[abe]

Received 20th June 2017,
Accepted 23rd August 2017

DOI: 10.1039/c7cp04144f

rsc.li/pccp

We report a detailed density functional theory (DFT) study in conjunction with extended X-ray absorption fine structure (EXAFS) experiments on the geometrical and local electronic properties of Cu adatoms and Cu(II) ions in presence of water molecules and of CuO nanoclusters on the CeO_2(110) surface. Our study of $(CuO)_{n(=1,2\&4)}$ clusters on CeO_2(110) shows that based on the Cu–O environment, the geometrical properties of these clusters may vary and their presence may lead to relatively high localization of charge on the exposed surfaces. We find that in the presence of an optimum concentration of water molecules, Cu has a square pyramidal geometry, which agrees well with our experimental findings; we also find that Cu(II) facilitates water adsorption on the CeO_2(110) surface. We further show that a critical concentration of water molecules is required for the hydrolysis of water on $Cu(OH)_2/CeO_2$(110) and on pristine CeO_2(110) surfaces.

1. Introduction

Cu/CeO_2 based catalysts have attracted great interest for heterogeneous catalysis because of their high catalytic activities for several processes, including NO_x reduction and both CO and hydrocarbon oxidation.[1] Similarly, CuO/CeO_2 mixed-oxide catalysts have been shown to have high activity and selectivity for CO oxidation in hydrogen-rich mixtures for CO clean-up in proton-exchange membrane fuel cells.[2] Despite several previous studies, there is, however, considerable uncertainty about the nature of Cu surface species in the catalytic material, which we aim to clarify in this paper by using a joint computational/experimental approach.

A crucial feature of the chemistry of CeO_2 is the variable valence of Ce, reduction of which from Ce(IV) to Ce(III) normally results in oxygen loss, but which can be effected by electron transfer from surface metal atoms.[3] The quantum chemical description of the strongly correlated electrons in the f-orbitals of Ce atoms, which become occupied when the Ce cations change their formal oxidation state from +4 to +3 is of primary importance, especially for understanding the fundamental properties and for their practical applications. In previous theoretical studies, density functional theory (DFT) with incorporation of Hubbard (U) and exchange energy (J) parameters, generally known as DFT+U, has been widely used.[4,5] For example, Branda *et al.* reported the interaction of Cu, Ag and Au with the CeO_2(111) surface.[6] In this work they concluded that the theoretical description using the DFT+U method is adequate to describe the interaction of Cu, Ag and Au on the CeO_2(111) surface. They used U = 5 for LDA+U and U = 3 and 5 for GGA+U calculations. They also argued that compared to Au/CeO_2(111), the interaction of Cu and Ag atoms on the CeO_2(111) surface is less sensitive to the DFT method used and the way the surface model is constructed. In their work they used the plane wave periodic techniques available in the VASP (Vienna Ab Inito Simulation Package) code and performed a comparative study of LDA+U and GGA+U. In a related study on Au/CeO_2(111), they used the hybrid HSE06 functional, in addition to LDA+U and GGA+U and found that the final description of the physical and chemical properties of these systems strongly depended on the choice of initial geometry.[7] Szabová *et al.* reported a detailed study on the thermodynamic, electronic and structural properties of Cu/CeO_2 surfaces and interfaces using the PBE+U method.[8] They used Cu atoms on stoichiometric and reduced CeO_2(111) surfaces and extended this study to Cu(111) on the CeO_2(111) surface to investigate the interfacial interactions. They concluded that the Cu adatom adopted the hollow site as the most stable site. They also investigated the electronic properties of the $Cu(111)/CeO_2$ interface and predicted substantial charge transfer in the

[a] *UK Catalysis Hub, RCaH, Rutherford Appleton Laboratory, Didcot, OX11 0FA, UK. E-mail: a.chutia@ucl.ac.uk, c.r.a.catlow@ucl.ac.uk*
[b] *Department of Chemistry, University College London, Gordon Street, London, WC1H 0AJ, UK*
[c] *School of Chemistry, University of Southampton, Southampton, 50718J, UK*
[d] *Diamond Light Source Ltd., Diamond House, Harwell Science and Innovation Campus, Didcot, Oxfordshire OX11 0DE, UK*
[e] *Cardiff Catalysis Institute, School of Chemistry, Cardiff University, Cardiff, CF10 3AT, UK*

† Electronic supplementary information (ESI) available. See DOI: 10.1039/c7cp04144f
‡ The co-ordinate files for all structures reported here can be obtained from DOI: 10.17035/d.2017.0040809826.

interfacial region, which could be related to the high catalytic activity of these systems. Cui *et al.* also reported the adsorption properties of transition metals, M, (M = Cu, Ag, Au) on the $CeO_2(110)$ surface.[9] They clearly showed charge transfer between the transition metals and the $CeO_2(110)$ surface resulting in Ce^{3+} and M cations being formed.[9] In a related work Tang *et al.* reported that structural distortion plays a significant role in understanding the local electronic properties due to the interaction of Cu, Ag, Au on $CeO_2(111)$ surface.[10] Additional studies of the electronic properties of precious metal adsorption on $CeO_2(111)$ surface include the work of Hernández *et al.* who showed that Au atoms in $Au/CeO_2(111)$ can adopt several oxidation states, depending on the site of their adsorption.[11] We should also note that in addition to the studies related to the adsorption and electronic properties of metal adatoms on CeO_2 surfaces, there are several studies on ceria bulk and surface properties, which provide insight into how intrinsic defects and doping in CeO_2 influences the electronic properties of bulk CeO_2.[12,13] Kehoe *et al.*, for example, reported doping of ceria by metal ions and showed that the dopant reduces the formation energy for oxygen vacancy formation energy, and the dopant tends to adopt a coordination environment close to that in its own native oxide.[13] There have also been a number of studies exploring the reaction mechanisms of industrially important reactions such as carbon dioxide activation and dissociation on $CeO_2(110)$ surface and the water-gas-shift reaction on $Au/CeO_2(111)$.[14,15] Many important chemical processes on surfaces, however, involve interaction with water molecules. In this regard, there has also been a number of interesting studies on the interaction of water molecules with CeO_2 surfaces.[16–19] Fronzi *et al.* for example, studied the structural features of adsorbed water on the stoichiometric and reduced $CeO_2(111)$ surface and predicted that a water molecule does not dissociate on the clean surface, but that it is thermodynamically favourable on the surface with O vacancies.[16] Han *et al.* also concluded that water molecules show molecular adsorption on the clean $CeO_2(111)$ surface and dissociative adsorption on $CeO_2(111)$ in the presence of single transition metal atoms.[17]

Despite this wide range of theoretical work on the surface chemistry of CeO_2,[20] considerable uncertainties remain regarding the key aspects of the interaction of catalytically important metals such as Cu on CeO_2 surfaces concerning their charge state, coordination and interaction with surface water. In this work we have employed density functional theory (DFT) in direct conjunction with extended X-ray absorption fine structure (EXAFS) to understand fundamental questions related to the adsorption sites of Cu on the $CeO_2(110)$ surface, their geometrical and local electronic properties, their substitution on the surface and in the bulk of CeO_2, their interaction with oxygen vacancies, the influence of their oxide clusters on the geometrical and electronic properties of CeO_2 surfaces and finally the electronic properties of the Cu(II) ion with varying concentrations of the water molecules. In the next section we present the theoretical and experimental methods used for this study, followed by the results of our detailed study of the properties of Cu adatoms on the CeO_2 surface. Our calculations are compared with the experimental results from our XAFS studies on Cu/CeO_2 (Cu nanoparticles synthesised in the reduced and oxidised state). We then present an account of $(CuO)_n$ clusters interacting with the $CeO_2(110)$ surface. These calculations were performed as the prepared materials for the experimental measurements used catalysts treated in air and hydrogen in order to change the type of species (CuO and Cu). Finally, we also report theoretical calculations on the geometrical and electronic properties of Cu(II) systems in the presence of water molecules. Our study leads to a detailed understanding of the structural and electronic properties of this important catalytic material.

2. Computational and experimental detail

2.1 Computational

We employed the Vienna Ab initio Simulation Package (VASP) to perform all the spin-polarized DFT+U calculations.[21–23] Theoretical studies have shown that the stability of CeO_2 surfaces is in the order of (111) > (110) > (100), and it is generally considered that the $CeO_2(110)$ surface is catalytically more active.[9,24] Therefore, for our studies we have focused on the latter surface. We used the projector augmented wave (PAW) method and the cut-off energy for the expansion of the plane-wave basis sets was set to 550 eV, which gave bulk energies converged to within 10^{-5} eV.[25] We chose a convergence criterion of 0.01 eV $Å^{-1}$ for structural optimizations. For all the calculations, the Perdew–Burke–Ernzerhof (PBE) version of generalized gradient approximation (GGA) was used to carry out geometry optimizations and the total energy calculations.[26] The ideal (110) surfaces were modelled by a 2×2 supercell with 9 atomic layers; the slab was cut from bulk CeO_2 with a theoretical lattice constant of 5.492 Å (Exp. 5.411 Å) and a k-point grid of $4 \times 4 \times 1$ was employed for all slab calculations. In the direction perpendicular to the surface, we used a vacuum gap of ~15 Å. In previous studies, it has been reported that the localization of electrons in f-orbitals in Ce ions is correctly represented by the Hubbard parameter U_{eff} = 5 eV.[24] In our studies we have used a U value of 5.0 for both Ce 4f-orbitals and Cu 3d-orbitals.[8,11,27,28] In our models, we placed the Cu atoms on both sides of the CeO_2 surface so as to nullify any spurious dipole moments that would be present in the single-sided system. Similar calculations were also performed on the CuO monomer, dimer and tetramer in order to understand the interaction between copper oxide and the CeO_2 surface.

The adsorption energies of these systems were calculated using:

$$E_{ad} = \{E_{X+CeO_2} - (E_{CeO_2} + 2 \times E_{adsorbate})\}/2, \quad (1)$$

where, E_{ad} is the adsorption energy, E_{X+CeO_2} is the energy of the system with the Cu or $(CuO)_{n(=1,2\&4)}$ adsorbed on $CeO_2(110)$ surface, E_{CeO_2}, is the energy of the pristine $CeO_2(110)$ surface, $E_{adsorbate}$ is the energy of an isolated Cu atom or $(CuO)_{n(=1,2\&4)}$ cluster. The charges on the various atoms were obtained using

the Bader charge analysis as implemented by Henkelman and co-workers.[29] The charge density difference, ρ_{diff}, was calculated by subtracting the sum of the charge densities of adsorbate $\rho_{adsorbate}$ and pristine geometry ($\rho_{Pristinesurface}$) of the surface of the same geometry from the total charge density (ρ_{total}) of the system *i.e.*

$$\rho_{diff} = \rho_{total} - (\rho_{Pristinesurface} - \rho_{adsorbate}) \quad (2)$$

For the calculations involving water molecules on Cu(II) systems, the adsorption was allowed on only one of the two surfaces. In these calculations the dipole moment, due to the adsorbed species, was accounted for using the methods implemented in VASP according to the procedures of Makov *et al.* and Neugebauer *et al.*[30,31] We used the Electronic and Structural Analysis (VESTA) package for the visualization of 3D and 2D charge density differences.[32,33]

2.2 Experimental

Synthesis. 1.5 wt% Cu/CeO_2 was synthesised based on a deposition–precipitation method.[34] An aqueous solution of $Cu(NO_3)_2$ (Sigma Aldrich) was prepared and the pH was brought to 8 by adding dropwise an aqueous solution of KOH (0.1 M). The solution was then heated at 70 °C and commercial CeO_2 (Ceria 60 Evonik) was added under vigorous stirring to the solution, keeping the slurry at 70 °C for 2 h. The obtained slurry was kept digesting for 24 h. The final catalyst was filtered, washed with warm water (70 °C) for several times until disappearance of nitrate and chloride species and finally dried at 120 °C under static air. After drying, two heat treatment procedures were followed. For the calcined catalyst the material was heat treated in static air at 450 °C for 1 h. For the reduced catalyst, the material was first calcined (at 450 °C for 1 h) and then reduced under H_2 flow (30 ml min^{-1}) at 150 °C for 1 h.

Characterisation. Cu K-edge XAFS (X-ray absorption fine structure) measurements, which give both the XANES (X-ray absorption near edge structure) and EXAFS regions, were performed at the Diamond Light Source, UK on beamline B18 with a fast-scanning Si(111) double crystal monochromator. The time resolution of the spectra reported was 5 min per spectrum (k_{max} = 14, step size 0.35 eV). Six fluorescence scans were acquired to improve the signal to noise level using a 9 element solid state germanium detector. EXAFS data analysis was performed using IFEFFIT with the Horae package (Athena and Artemis).[35,36]

3. Results and discussion

We first discuss the results of both our computational and experimental analysis of Cu on the CeO_2(110) surface before examining the behaviour of Cu^{2+} ions and of oxide clusters and the role of water.

3.1 XAFS studies on Cu on Ceria

The Cu K-edge XANES spectra of the Cu/CeO_2 reduced and calcined samples with the reference samples Cu^0, Cu(I)oxide and Cu(II)oxide are shown in Fig. 1. Both samples show features

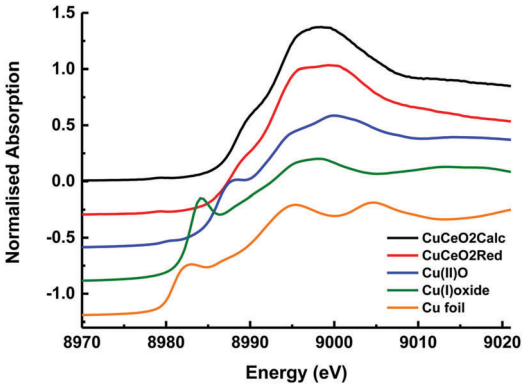

Fig. 1 Normalised XANES spectra of Cu/CeO_2 calcined (black), Cu/CeO_2 reduced (red), and the reference materials CuO (blue), Cu_2O (green) and Cu foil (orange).

similar to Cu(II)O indicating a Cu^{2+} oxidation state. However, the 1s → $4p_z$ transition which appears at 8988 eV for CuO is less pronounced, suggesting that unlike CuO these samples are not in a square planar coordination.[37] The addition of an axial ligand around a Cu^{2+} centre has been shown to reduce the intensity of the 1s → $4p_z$ transition, and we propose that the Cu in these samples is in either a distorted octahedral or square pyramidal environment.[38,39]

The k^2 weighted Fourier transform EXAFS data for the reduced and calcined samples and the calculated fitting parameters are shown in Fig. 2 and Table 1. The data were fitted using two oxygen scattering paths. The fit of the calcined sample resulted in a coordination number of four for the first Cu–O path with a distance of 1.940 Å, and a distance of 2.390 Å for the second O-scattering path. In the Fourier transform of the EXAFS data, Fig. 2, there are subtle features at longer distances suggestive of scattering from a heavier element such as Cu, with which features in the $\chi(k)$ data are also consistent. As these features are subtle in comparison to that of bulk CuO, it would suggest that the samples measured here are small clusters. Similarly, for the reduced sample, a coordination number of four was obtained for the first Cu–O path with a Cu–O distance of 1.940 Å and coordination number of two with a Cu–O distance of 2.390 Å for the second. The EXAFS fitting correlates well with the assumption from the XANES spectra that the Cu is in a distorted octahedral or square pyramidal environment, having two different Cu–Cu distances and an overall coordination of around six.

In the next stage of our study we perform DFT calculations to interpret the experimental findings on coordination number of Cu and its local geometry, which is then extended to understand how the O-atom environment around Cu influences its electronic properties.

3.2 Cu adatom on CeO_2(110) surface

First, we investigate the geometry and electronic properties of adsorbed Cu adatoms on the CeO_2(110) surface. The adsorption of a single Cu atom is evaluated in four different sites namely, (1) on top of the O-atom (O_{top}), (2) on-top of the Ce-atom (Ce_{top}),

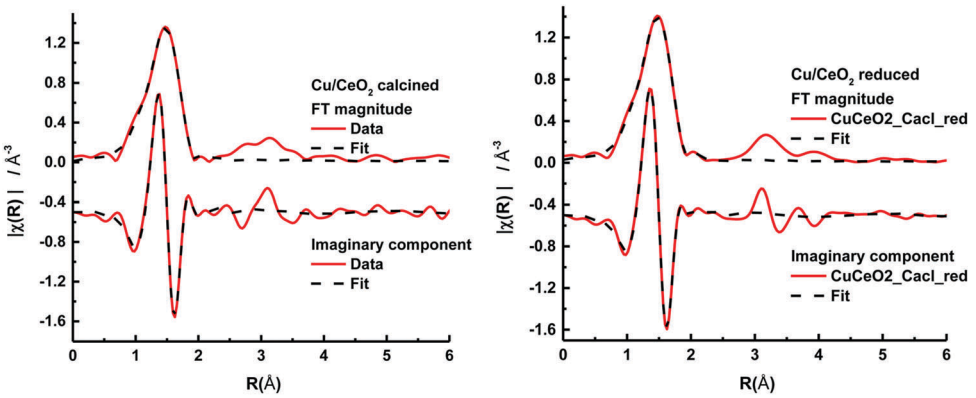

Fig. 2 Magnitude and imaginary components of the k^2 weighted Fourier transform for the EXAFS data of the Cu K-edge of the calcined and reduced Cu/CeO_2 samples.

Table 1 EXAFS fitting parameters for the calcined and reduced Cu/CeO_2 samples. Fitting parameters: $S_0^2 = 0.72$ calculated using a Cu foil standard; fit range $2.5 < k < 10.9$, $1 < R < 3$; number of independent points: 10.4

Sample	Abs–Sc	CN	R (Å)	σ^2	E_f (eV)	R_{factor}
Cu/CeO_2 calcined	Cu–O	4.8 ± 0.7	1.94 ± 0.01	0.005 ± 0.002	1 ± 2	0.02
	Cu–O	1 (set)	2.39 ± 0.09	0.01 ± 0.02		
Cu/CeO_2 reduced	Cu–O	5.2 ± 0.5	1.949 ± 0.009	0.006 ± 0.001	1 ± 1	0.006
	Cu–O	1 (set)	2.4 ± 0.1	0.03 ± 0.03		

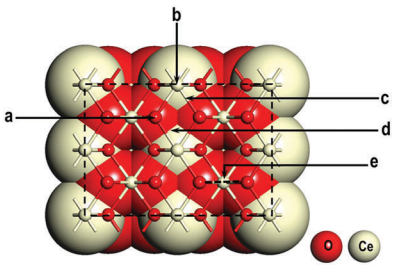

Fig. 3 The adsorption of Cu adatoms were investigated on (a) top of O-atom, (b) top of Ce-atom, (c) O–Ce bridge, (d) the four-fold hollow site and (e) long-bridge site of $CeO_2(110)$ surface. The periodic boundary of the 2 × 2 model is shown with dotted lines. The first two layers are shown in ball and sticks and lower layers are shown in van der Waals spheres. The O atoms are shown in red and Ce atoms in canary colours as indicated in the key.

(3) O–Ce bridge site ($O–Ce_{bdg}$) and (4) on the four-fold hollow site (4-fold_{hollow}) (see Fig. 3).

Geometries. The optimized geometries are shown in Fig. 4. After geometry optimization, the Cu adatom has moved to the long bridge site for the O_{top} and $Ce–O_{bdg}$ systems. These two geometries after geometrical optimization are similar but not identical. In both cases, the Cu atom has moved to the long bridge site after geometry optimization (Fig. 4(a and c)); and O_{top} and $Ce–O_{bdg}$ systems can also be thought of as ''top-long-bridge'' and ''bridge-long-bridge'' configurations, respectively. These results are consistent with previous theoretical studies.[9] We see that in these two systems, the oxygen atoms close to the Cu adatom rise up towards the Cu-atom disturbing the planarity of the surface. For the Ce_{top} system the Cu atom moves away from the Ce atom (by 3.303 Å), which indicates a weak interaction between Cu and the CeO_2 surface. In the case of the 4-fold_{hollow}, Cu remains close to the surface. However, as shown in Table 2, an analysis of the bond lengths shows that overall Ce–O distances in the Cu adsorbed systems are comparable with those of the pristine $CeO_2(110)$ surface. We also found that the Cu–O bonds are relatively shorter for O_{top} and $O–Ce_{bdg}$ as compared to 4-fold_{hollow} site, which indicates a stronger interaction between the Cu atom and the $CeO_2(110)$ surface for these locations.

Energetics of Cu adsorption on the $CeO_2(110)$ surface. In the next step, we investigate the adsorption energy of Cu adatoms on the above four configurations of Cu on $CeO_2(110)$ surface. As shown in Table 2, the adsorption energy increases in the order: $O_{top} < O–Ce_{bdg} < 4\text{-fold}_{hollow} < Ce_{top}$, *i.e.*, a Cu atom is most stable in the O_{top} position. However, as mentioned in our discussion on local geometry above, it is interesting to note that after geometry optimization, O_{top} and $O–Ce_{bdg}$ have similar geometries *i.e.*, the Cu atom occupies a position in the long-bridge site inbetween two oxygen atoms. But the adsorption energy of O_{top} is −0.212 eV lower than the $O–Ce_{bdg}$ system. To clarify the underlying reasons for the difference in their adsorption energy and hence in their stability, we analyze the atom projected partial density of states (PDOS). As shown in Fig. 5(a and b) the PDOS for both O_{top} and $O–Ce_{bdg}$ configuration in terms of orbital-interactions appear similar. However, in the case of O_{top}, the contribution of O p orbitals (approximately from −1.5 eV to 0 eV, marked by blue circles) is comparable to the highly-localized Cu d-orbitals, which completely overlap with each other; but in the case of Cu on the $O–Ce_{bdg}$ site, the contribution of O is lower than the Cu d-orbitals, so that the interaction of the nearby O-atoms with the Cu-atom is

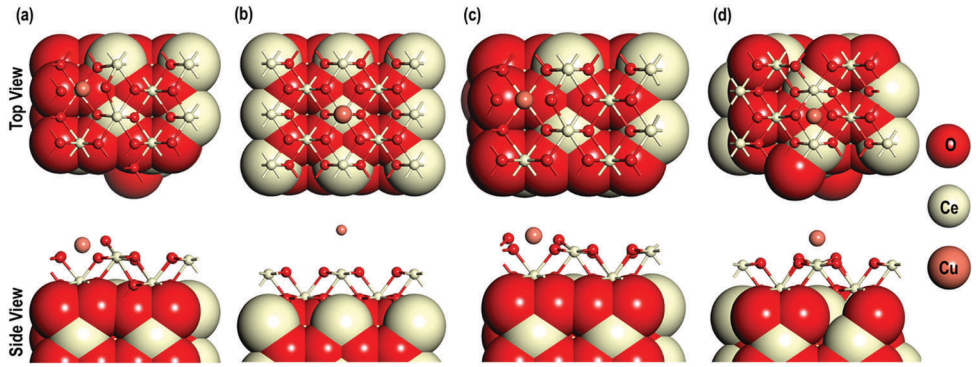

Fig. 4 Optimized structures of Cu on (a) top of O, (b) top of Ce, (c) Ce–O bridge and (d) four-fold hollow sites. The first two layers are shown in ball and sticks and lower layers are shown in van der Waals spheres. The O atoms are shown in red, Ce atoms in canary and Cu atoms as congo pink colours as indicated in the key.

Table 2 Bond lengths for Ce–O on bulk and on the surface of pristine CeO_2(110) surface and on CeO_2(110) surface with Cu on-top O-atom (O_{top}), on top of Ce-atom (Ce_{top}), on Ce–O bridge (Ce–O_{bridge}) and on the four-fold hollow site (4-$fold_{hollow}$)

		Bond lengths (Angs)				
System		$(Ce–O)_{blk}$	$(Ce–O)_{srf}$	Cu–O	Cu–Ce	E_{ad} (eV)
Pristine	—	2.378	2.341	—	—	—
Cu on	O_{top}	2.376	2.342	1.773	—	−3.236
	Ce_{top}	2.378	2.343	—	3.303	−0.101
	O–Ce_{bridge}	2.377	2.337	1.767	—	−3.024
	4-$fold_{hollow}$	2.377	2.338	1.961	—	−1.061

stronger for the O_{top} case as compared to the O–Ce_{bdg} case. Other than that the overall signatures due to Cu(s, p and d) and O(s and p) for both O_{top} and O–Ce_{bdg} cases are similar. To gain a more detailed picture of the interaction of the molecular orbital, we zoomed-in the PDOS (see Fig. 5(c and d)). At around −6 eV to −5 eV region (marked by green circles) an interesting contribution of a low-lying Cu p-orbital for the O_{top} case are seen, which overlaps with the O s-orbital signatures leading to stronger bonding between the Cu-atom and nearby O-atoms. Similar contributions for the O–Ce_{bdg} configuration are, however, not seen. This analysis clearly suggests that despite their similar geometries the O_{top} system is more stable as compared to O–Ce_{bdg} due to the stronger hybridization between Cu and surface O atoms in the former.

Electron transfer from the Cu atom to the CeO_2(110) surface. After determining the most stable configuration for the adsorption of a Cu-atom, we extended our investigation to the electron transfer for this system, focusing on the O_{top} model. Here, we performed a comparative study on the f-orbital contribution of Ce in pristine CeO_2(110) and on the O_{top} model using the PDOS. Before the adsorption of the Cu atom on CeO_2(110) surface, the highest contribution of f-orbital signatures due to Ce atoms are above the E_F. Traces of the f-orbital signatures are also seen below −3 eV to −1 eV. However, with the adsorption of the Cu

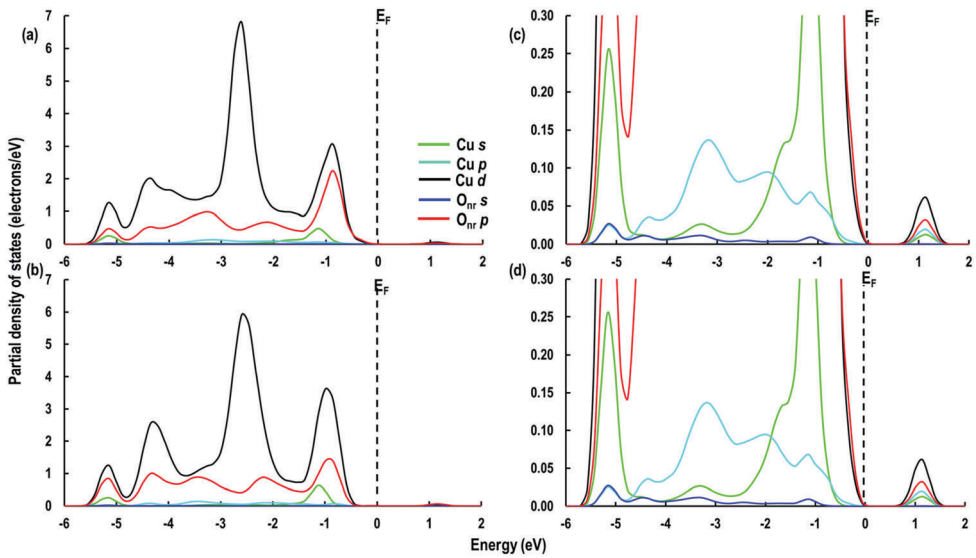

Fig. 5 PDOS for (a) Cu on-top of O, (b) Cu on O–Ce bridge sites. The zoomed-in PDOS for (c) Cu on-top of O, (d) Cu on O–Ce bridge sites for analysing the contribution of low-lying orbitals. The subscript "nr" refers to the oxygen atom close to the Cu ion.

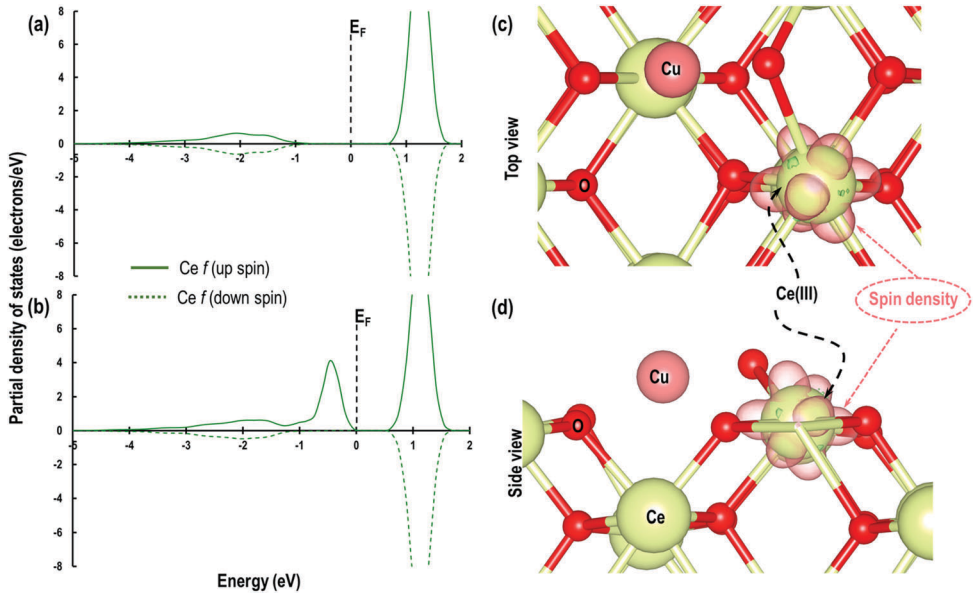

Fig. 6 PDOS for Ce f-orbitals for Ce atoms in (a) pristine and (b) Cu on top-long-bridge site of CeO_2(110). The Fermi energy (E_F) is shifted to zero and it is marked by a dashed line. (c) Side view and (d) top-view of isosurface of 0.006 e Å^{-3} for electron spin-density around the reduced Ce atom.

in O_{top} model there is an appearance of an f-orbital signature just below E_F (Fermi energy), clearly showing that the Ce(IV) atom is reduced to Ce(III) due to electron transfer (Fig. 6(a and b)). We also visualized the isosurface of electron spin densities for the O_{top} model, which also clearly shows electron gain around the Ce-atom on the CeO_2(110) surface (see Fig. 6(c and d)). We further illustrated the electron transfer by calculating Bader charges, which give $+2.385e^-$, $-1.196e^-$ and $+0.454e^-$ for Ce, O and Cu atoms respectively on the CeO_2(100) surface. The Bader charge on the reduced Ce is seen to be $+2.102e^-$, which clearly shows electron gain.

Cu(II) on the surface and in the bulk. In the above section we discussed the geometrical and electronic properties of Cu-adatoms on the CeO_2(110) surface. However, as described in the Experimental section, Cu appears to be present predominantly as Cu(II). To construct models of CeO_2 with Cu(II) incorporated, we first substitute a Ce atom with a Cu^{2+} ion either on the surface using the CeO_2(110) slab representation or in the bulk material and created an oxygen vacancy for charge compensation. We refer to the Cu^{2+} ions replacing surface and bulk ceria as Cu_{srf} and Cu_{blk} respectively.

The optimized structures show interesting geometrical properties. In the Cu_{srf} model, the Cu adopts a square-planar structure with the nearby O-atoms (Fig. 7(a and b)). The four Cu–O bond distances are: 1.918 Å (O_1), 1.949 Å (O_2), 1.940 Å (O_3) and 1.967 Å (O_4) (Fig. 7(a)), which agree with previous theoretical findings.[8] In the case of Cu_{blk} also, the Cu atom adopts a square-planar structure with four close O-neighbours at a distance of 1.965 Å (O_1), 1.950 Å (O_2), 1.956 Å(O_3) and 1.950 Å (O_4). (Fig. 7(c)). These distances are also comparable with the bond distances

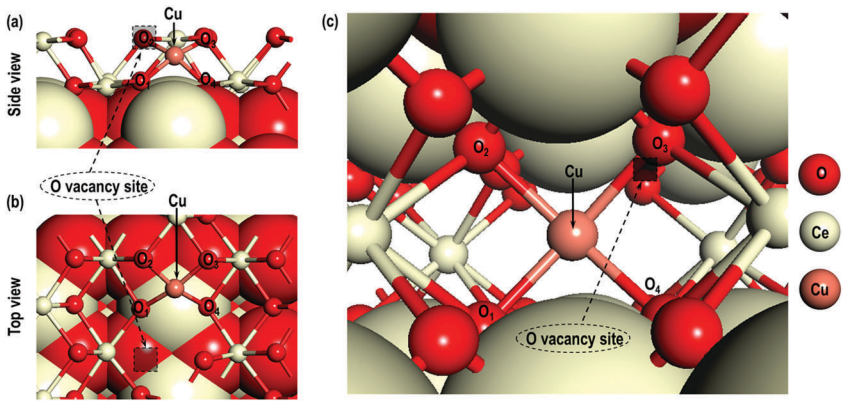

Fig. 7 Optimized structures of Cu on the surface of CeO_2(110) surface (Cu_{srf}) with an O-vacancy (a) side-view and (b) top-view and (c) side-view for Cu in the bulk (Cu_{blk}). The position of the O vacancy is marked by a dotted-filled black squares. Two layers directly interacting with the Cu atoms are shown in ball and sticks and rest of the atomic layers are shown in van der Waals spheres. The O atoms are shown in red, Ce atoms in canary and Cu atoms as congo pink colours as indicated in the key.

from our EXAFS measurements. However, the coordination number does not agree with that derived from the EXAFS. As a Cu(II) centre has a d^9 configuration, these models contain unpaired electrons. On visualizing the calculated spin density of these systems, we see that it is highly localized around the Cu centres and nearby O-atoms in both bulk and surface substitution positions. The shape of this spin density indicates that there is bonding between Cu d and O p-orbitals (see ESI†).

3.3 $(CuO)_{n(=1,2\&4)}$ clusters on $CeO_2(110)$ surface

Clearly the calculated geometries of the Cu centres in the surface and bulk using the simple substitution models do not match well with the experimental EXAFS measured parameters for the Cu environments. Therefore, we performed a study of the interaction of $(CuO)_{n(=1,2\&4)}$ clusters on the $CeO_2(110)$ surface. Initially, we have attempted to identify the stable location for CuO on the $CeO_2(110)$ surface. Two different configurations: (a) Cu atom of Cu–O on the four-fold hollow site and O on top of the Ce atom, which gives a natural continuation of the underlying lattice (Conf.1) and (b) the Cu atom of Cu–O on top of the Ce atom and O in the long-bridge site (Conf.2), which places the O atom far away from surface O anions but does put the Cu cation close to a surface Ce, which is expected to lead to a significant repositioning of the Cu–O unit on relaxation. For convenience, the top and side views of the above two configurations have been shown in Fig. 8(a and b). In the fully relaxed structure Conf.1, the Cu–atom forms a bond with one of the two nearby O–atoms with a coordination number of two for Cu (Fig. 8(b)) while Conf.2 attains a vertical Ce–O–Cu geometrical configuration (Fig. 8(d)). The bond distances around the Cu–O are summarized in Table 3. We see that in both configurations, the Cu–O bond distances are in the range of 1.726–1.886 Å, which are shorter than the experimentally observed bond distances (1.940–2.390 Å), the probable reason for which can be attributed to the environment around the Cu and O atoms. The adsorption energy of Conf.1 (−2.423 eV) is more negative than Conf.2 (−1.170 eV) implying higher stability of Conf.1. Therefore, in the next step, on the basis of the optimized geometry and energetic favorability of Conf.1 we build $(CuO)_{2\&4}$ clusters on the $CeO_2(110)$ surface with Cu atoms closer to surface O–atoms and O-atoms closer to the surface Ce-atoms.

In the $(CuO)_2/CeO_2(110)$ system both Cu–atoms have a coordination number of two, while in the case of the $(CuO)_4/CeO_2(110)$ system there are two types of Cu-atoms with coordination number of three and two others with four. The optimized structures are shown in Fig. 8(e and f). In the $(CuO)_2/CeO_2(110)$ system, we see that there are different sets of Cu–O bond distance *i.e.*, within the $(CuO)_2$ cluster the average Cu–O bond distance is 1.854 Å and the average bond distance between Cu of $(CuO)_2$ from the surface O-atoms is 1.966 Å. On the other hand in the $(CuO)_4/CeO_2(110)$ system, the Cu–O bond distances are 1.883 Å from the CeO_2 surface. In the first layer above the $CeO_2(110)$ surface, the CuO bond distances are 2.191 Å. The distance from the first to the second layer is either 1.891 Å or 1.934 Å. In the uppermost layer, the Cu–O bond distances are 1.912 Å and 1.895 Å, which shows that that the Cu–O bond distances are determined by the number of surrounding Cu and O atoms. Overall, we see a monotonic increase in Cu–O bond distances with increase in $(CuO)_{n(=1,2,4)}$ cluster size and the bond distances are comparable with those of the experimental Cu–O bond distances as reported in Table 1. Furthermore, on considering the Ce–O bond distances on the surface or in the bulk, we find that the average bond distances are comparable. However, it is interesting to note that near the $(CuO)_{n(=1,2\&4)}$ cluster, minor expansion and contraction of the Ce–O bond distances take place. We have also calculated the adsorption energies for each cluster relative to the same gas-phase species and find that the adsorption energy per Cu–O unit decreases with cluster size so that for Cu–O E_{ad} = −2.417 eV, for $(Cu–O)_2$ E_{ad} = −1.410 eV and for $(Cu–O)_4$ E_{ad} = −1.291 eV.

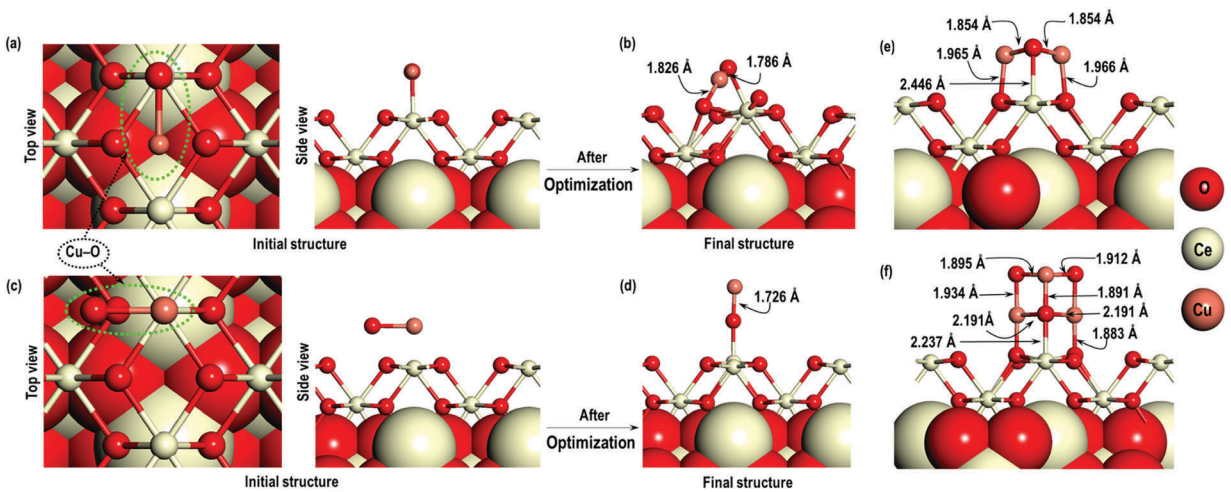

Fig. 8 Side view and top view of a CuO diatomic cluster with (a) O on top of a Ce atom and Cu in the four-fold hollow site (Conf.1) and (b) Cu on top of a Ce atom and O in the long-bridge site (Conf.2). Optimized structure of (c) Conf.1, (d) Conf.2, (e) $(CuO)_2$ cluster on $CeO_2(110)$ and (f) $(CuO)_2$ cluster on $CeO_2(110)$. The first two layers are shown in ball and sticks and lower layers are shown in van der Waals spheres. The O atoms are shown in red, Ce atoms in canary and Cu atoms as congo pink colours as indicated in the key.

Table 3 The average bond distances for Ce–O in the bulk ($(Ce–O)_{blk}$), on the surface ($(Ce–O)_{srf}$), Cu–O bond distances in the $(CuO)_{n(=1,2\&4)}$ ($(Cu–O)_{clstr}$), Cu–O bond distances for Cu of $(CuO)_{n(=1,2\&4)}$ cluster and O of the $CeO_2(110)$ surface $Cu_{clstr}–O_{srf}$ and O of the $(CuO)_{n(=1,2\&4)}$ cluster and Ce of the $CeO_2(110)$ surface

	Average bond distances (Å)				
System	$(Ce–O)_{blk}$	$(Ce–O)_{srf}$	$(Cu–O)_{clstr}$	$Cu_{clstr}–O_{srf}$	$O_{clstr}–Ce_{srf}$
$(Cu–O)_{Conf.1}/CeO_2(110)$	2.378	2.339	1.726	—	2.112
$(Cu–O)_{Conf.2}/CeO_2(110)$	2.381	2.301	1.786	1.826	2.139
$(Cu–O)_2/CeO_2(110)$	2.377	2.338	1.854	1.966	2.446
$(Cu–O)_4/CeO_2(110)$	2.377	2.370	2.004	1.883	2.237

Finally, we visualize the electronic charge density difference using:

$$\rho_{diff} = \rho_{total} - (\rho_{CeO_2} - \rho_{(CuO)_{n(=1,2\&4)}}) \quad (3)$$

where, ρ_{diff} is the charge density difference, ρ_{total} is the charge density of the $(Cu–O)_{n(=1,2\&4)}/CeO_2(110)$ system, which constitutes of $CeO_2(110)$ surface and $(Cu–O)_{n(=1,2\&4)}$ clusters, ρ_{CeO_2} is the charge density of the $CeO_2(110)$ surface without the $(Cu–O)_{n(=1,2\&4)}$ clusters and $\rho_{(CuO)_{n(=1,2\&4)}}$ is the charge density of the $(Cu–O)_{n(=1,2\&4)}$ clusters in isolation. These density difference plots show that, due to the presence of the $(CuO)_{n(=1,2,4)}$ clusters, there is charge accumulation close to the $CeO_2(110)$ surface (blue lobes in Fig. 9(a–c)). To confirm this finding we then calculated the Bader charge distribution on the Ce atoms layer by layer through the simulation slab, (see Fig. 9(d)), which shows that on the uppermost layers, close to these clusters, there is accumulation of electron density as compared to the atoms in the bulk.

3.4 Cu(II) in the presence of water molecules

The above study shows closer agreement of Cu–O bond distances with experimental findings but to reproduce the Cu environment found by experiment further investigation is required. We now extend our study to the systematic investigation of the influence of the O-environment around the Cu(II) atom on the geometrical and electronic properties, which is achieved by introducing hydroxide groups and water molecules, which are likely to be present in the synthesized material. Cu(II) is modelled by introducing two OH groups to be bonded to the Cu atom and the $Cu(OH)_2$ system is placed in close proximity with four other oxygen atom in the long bridge site (Fig. 10(a and b)). Subsequently this system of two OH groups bonded to the Cu atom on the surface of $CeO_2(110)$ surface will be referred to as the "$Cu(OH)_2$ system". We note that there is no need for a charge compensating oxygen defect in the ceria surface for this model.

For comparative purposes, similar calculations were carried out placing a Cu-atom in close proximity to four oxygen atoms in the long-bridge site with two water molecules in close proximity (Fig. 10(c)), which will allow assessment of the influence of Cu oxidation state on the calculated geometries. After optimization the $Cu(OH)_2$ system forms Cu(II) in a square planar structure (with coordination number = four) while the structure in Fig. 10(c) calculation gives a linear –OCuOH structure (with coordination number = two). In the case of the latter system with two water molecules, we see interesting surface restructuring followed by hydrolysis of a water molecule and the adsorption of OH to a nearby Ce-atom on the $CeO_2(110)$ surface is also seen. The Cu-atom forms bonds with one of the O-atoms bonded to an H-atom from the hydrolyzed water molecule, which loses its planarity with the rest of the CeO_2 surface. The average Cu–O bond distances in this systems is calculated to be 1.813 Å. In the $Cu(OH)_2$ system, however, no such surface restructuring is observed and the Cu–O bond distance is 1.940 Å.

We also investigated whether the adsorption of water molecules on the $Cu(OH)_2$ system influences the overall geometry generally and the coordination number of Cu with respect to O-atoms in particular, for comparison with the EXAFS data. For these calculations we use the fully relaxed geometry of the $Cu(OH)_2$ system described above and then include one, five and finally fifteen water molecules to represent solvent remaining on the surface of the material from adsorption of water from the environment (Fig. 11(a–c)). The first water molecule was placed with O coordinating to Cu and additional water molecules were introduced so as to form a H-bonding network. Various bond distances are summarized in Table 4. We see from the table that the overall Ce–O bond lengths on the $CeO_2(110)$ surface and in the bulk of $CeO_2(110)$ surface do

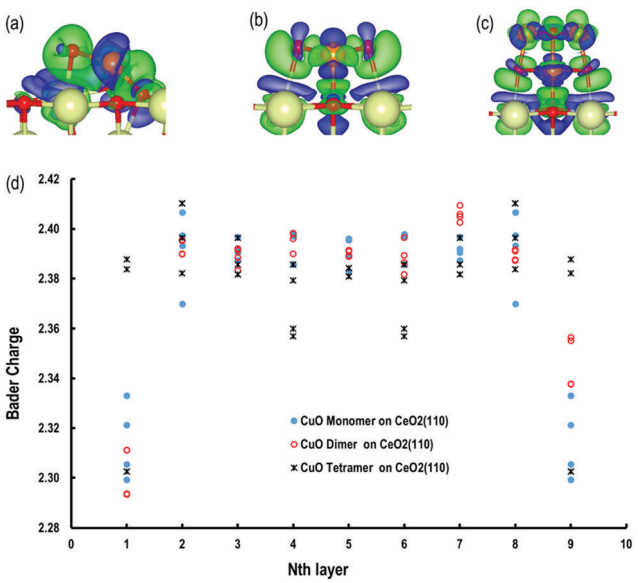

Fig. 9 Electron charge density difference of (a) Conf.1, (b) $(CuO)_2$ and (c) $(CuO)_4$ clusters and (d) Bader charge distribution on Ce atoms by layers.

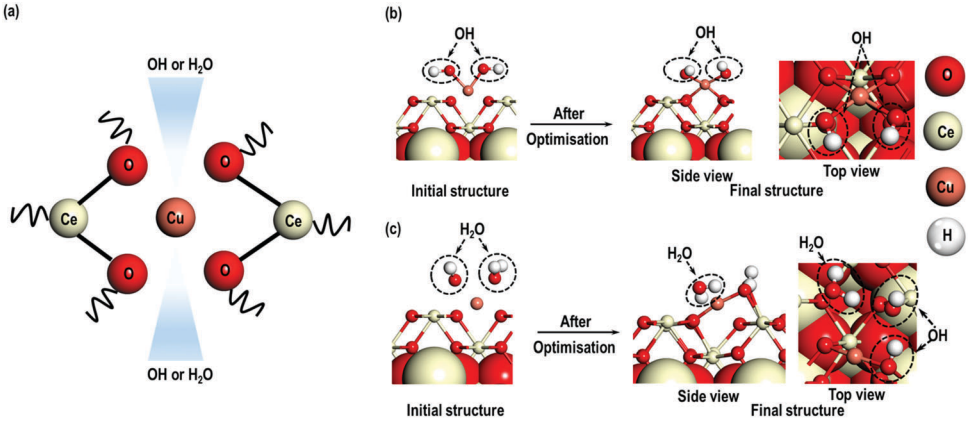

Fig. 10 (a) A schematic representation of initial models with an octahedral O-atom environment around a Cu on the long-bridge site of CeO_2(110) surface. The curly lines represents other surface atoms. (b) Initial and final structure of $Cu(OH)_2$ and (c) initial and final structure of $Cu(H_2O)_2$ on the long-bridge site. The first two layers are shown in ball and sticks and lower layers are shown in van der Waals spheres. The O atoms are shown in red, Ce atoms in canary, Cu atoms as congo pink and H atoms in white colours as indicated in the key.

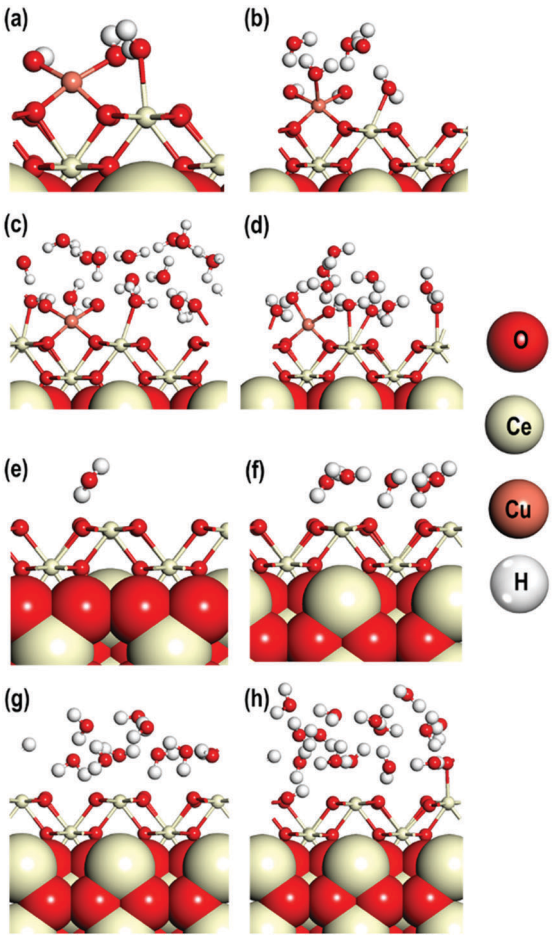

Fig. 11 Cu(II) on CeO_2(110) surface in presence of (a) 1, (b) 5 and (c) 15 water molecules and (d) Cu(II) in the long-bridge site and relaxed in presence of 10 water molecule. (e) 1, (f) 5, (g) 10 and (h) 15 water molecules on pristine CeO_2 (110) surface. The first two layers are shown in ball and sticks and lower layers are shown in van der Waals spheres. The O atoms are shown in red, Ce atoms in canary, Cu atoms as congo pink and H atoms in white colours as indicated in the key.

not change significantly. The Ce–O bond distances are only slightly longer near the $Cu(OH)_2$ group of atoms. Moreover, the calculated Cu–O bond distances are close to the experimentally reported value of 1.940 Å for both calcined and reduced Cu/CeO_2 systems (see Table 1). It is interesting to note that Cu has a coordination number of five, only in the case of five water molecules, which resembles a square pyramidal structure as seen in our experimental findings (Section 3.1). As shown in Table 4, four of these Cu–O bond lengths are 1.996 Å and the other Cu–O distance is 2.307 Å, which is due to the adsorbed water on Cu. These calculated Cu–O distances are in agreement with the experimental findings. In all other cases, a coordination number of four is seen, which clearly shows that there is an optimum number of water molecule favouring a higher coordination number due to hydrogen-bonding between nearby water molecules. We may attribute this behavior to the fact that when the number of water molecules is higher, the intermolecular H-bonding is stronger, so water molecules drift away from the Cu-atom to form water clusters, leading to a Cu–O coordination number of only four.

We also performed additional calculations to confirm whether the initial geometry of the $Cu(OH)_2$ system influences the final coordination number of the Cu-atom. Here, the Cu-atom bonded to two OH groups is placed in close proximity to four O-atoms on the long-bridge site of the CeO_2(110) surface along with 10 water molecules and is then fully relaxed (Fig. 11(d)). In the fully relaxed geometry, the Cu-atom maintains a coordination number of four. But it is interesting to note that in the optimized structure, the Cu-atom is coordinated to one H_2O molecule, which is formed by proton-transfer to one of the OH groups bonded to the Cu(II) ion from a neighboring water molecule, which leads to the adsorption of an OH group to a Ce-atom on the CeO_2(110) surface. We also see that three of the other nine water molecules adsorb on the CeO_2(110) surface and the other six water molecules set up an H-bonding network to form a water cluster. In the other models with one, five and fifteen water molecules, we do not find dissociation of water molecules.

Table 4 Coordination number (CN) around the Cu(II) ion and the average bond distances for Ce–O in the bulk ($(Ce–O)_{blk}$), on the surface ($(Ce–O)_{srf}$), Ce–O distance close to the Cu(II) ion ($(Ce–O)_{Cu}$), Cu–O distances close to the Cu(II) ion ($Cu–O_{nr}$), distance between O of adsorbed H_2O and Ce on the surface and distance between the adsorbed H_2O on Cu(II) ion ($Cu–H_2O$)

		Bond distances (Å)					
System	CN around Cu	$(Ce–O)_{srf}$	$(Ce–O)_{blk}$	$(Ce–O)_{Cu}$	$Cu–O_{nr}$	$Ce–H_2O_{ad}$	$Cu–H_2O$
Cu + 2 water mol.	2	2.338	2.378	2.510	1.814	2.753	—
$Cu(OH)_2$	4	2.317	2.378	2.519	1.940	—	—
$Cu(OH)_2$ + 1 water mol.	4	2.306	2.378	2.447	1.938	2.628	—
$Cu(OH)_2$ + 5 water mol.	5	2.316	2.378	2.483	1.996	2.561	2.307
$Cu(OH)_2$ + 15 water mol.	4	2.340	2.378	2.462	1.947	2.591	—

Furthermore, we also performed calculations for one, five, ten and fifteen water molecules on pristine surfaces for a comparison with that of the $Cu(OH)_2/CeO_2$ system (Fig. 11(e–h)). These calculations reveal that, in general, water molecules tend to cluster together by forming H-bonds. However, at a very high concentration of fifteen water molecules (Fig. 11(h)) dissociation of water molecules can be seen. In all cases, the water molecules are arranged in such a fashion as to form H-bonds with the surface O-atoms of CeO_2 or among themselves. From the above comparison of water molecule in pristine $CeO_2(110)$ surface and $Cu(OH)_2/CeO_2(110)$ surface we find that the latter $Cu(OH)_2$ system facilitates adsorption of water molecules on the $CeO_2(110)$ forming $Ce–OH_2$ bonds ranging from 2.591 to 2.753 Å (see Table 4) and dissociation of water molecules take place at a lower concentration than for pristine $CeO_2(110)$.

In the next phase of this study, we analyze in more detail the nature of the interaction of water molecules on the surface of $CeO_2(110)$, which requires calculation of the charge density difference using, in this case, the equation:

$$\rho_{diff} = \rho_{total} - (\rho_{CeO_2+Cu(OH)_2} - \rho_{(H_2O)_{n(=1,5\&15)}}) \quad (4)$$

Here, ρ_{diff} is the charge density difference, ρ_{total} is the charge density of the system, which constitutes of $CeO_2(110)$ surface, $Cu(OH)_2$ and water molecules, $\rho_{CeO_2+Cu(OH)_2}$ is the charge density of the $CeO_2(110)$ surface with $Cu(OH)_2$ system without water molecule and $\rho_{(H_2O)_{1,5\&15}}$ is the density of one, five or fifteen water molecules. For clarity, we generate 2D contour maps for the electron charge density differences for the uppermost layer consisting of Ce and O atoms directly interacting with the H_2O molecules in the $Cu(OH)_2$ systems. As shown in Fig. 12(a–c), for further clarity we have also labeled the Ce and O atoms of the $CeO_2(110)$ surface. The variation in the peak heights may be related to charge polarization due to the presence of water molecules. From this analysis we conclude that with an increase in the number of water molecules, there is a redistribution of charges on the surface of $CeO_2(110)$ surfaces especially around the H_2O molecules. It is also worth noting that the contour around the Ce atom marked as Ce′ in Fig. 12(a–c) is different for the $Cu(OH)_2$ system with five H_2O molecules (Fig. 12b), which may be related to the fact that in close proximity to this Ce atom in addition to one of the OH of $Cu(OH)_2$, there is another water molecule, while in the $Cu(OH)_2$ systems with one and fifteen water molecules, other than the OH of $Cu(OH)_2$, there are no other water molecules. The analysis of PDOS of Ce atoms on which water molecules are adsorbed shows no direct charge transfer between water molecules and the CeO_2 surface.

We have also analyzed the PDOS for the Cu-atom and one of the two O-atoms of OH group to understand how the increase in the number of water molecules influences the local electronic properties of the Cu(II) ion in the $Cu(OH)_2$ systems. We find that on increasing the number of water molecules from one to five and fifteen, the overall nature of up-spin and down-spin orbital contribution due to Cu s, O p and Cu d is comparable (see Fig. 13(a–c)). However, interesting changes in the contribution of these orbitals can be seen when we focus on the contribution of O p and Cu d-orbital signatures around −8 eV to −6 eV where in the case of $Cu(OH)_2$ system with five water molecules, the down-spin O p-orbital is broader than the other two cases (see Fig. 13(d and e)). In the $Cu(OH)_2$ system with one water molecule, the up-spin O p-signatures are not as broad as $Cu(OH)_2$ with five water molecules and in the $Cu(OH)_2$ system with fifteen water molecule the up-spin O p orbitals have two pronounced peaks. In addition another notable feature is seen at the top of the valence band, around −1 eV (green dotted circle in Fig. 13(a–c)) where, in the case of the $Cu(OH)_2$ system with five water molecules the Cu d-orbitals becomes particularly broad,

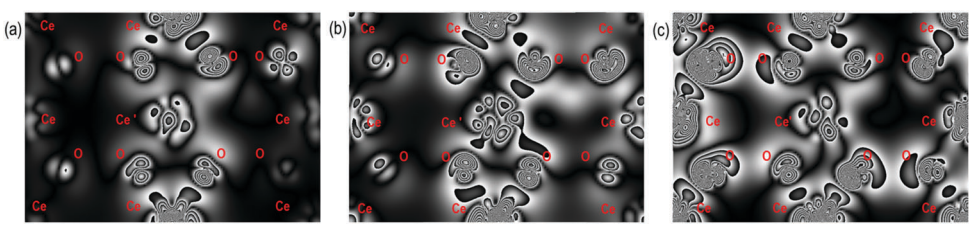

Fig. 12 A 2D contour representation of charge density difference of the top layer of CeO_2 (110) surface interacting with (a) 1, (b) 5 and (c) 15 water molecules in $Cu(OH)_2–CeO_2$ systems, which clearly shows that with increase in the number of water molecules, there is a redistribution of charges on the surface of $CeO_2(110)$ surfaces especially around the H_2O molecules.

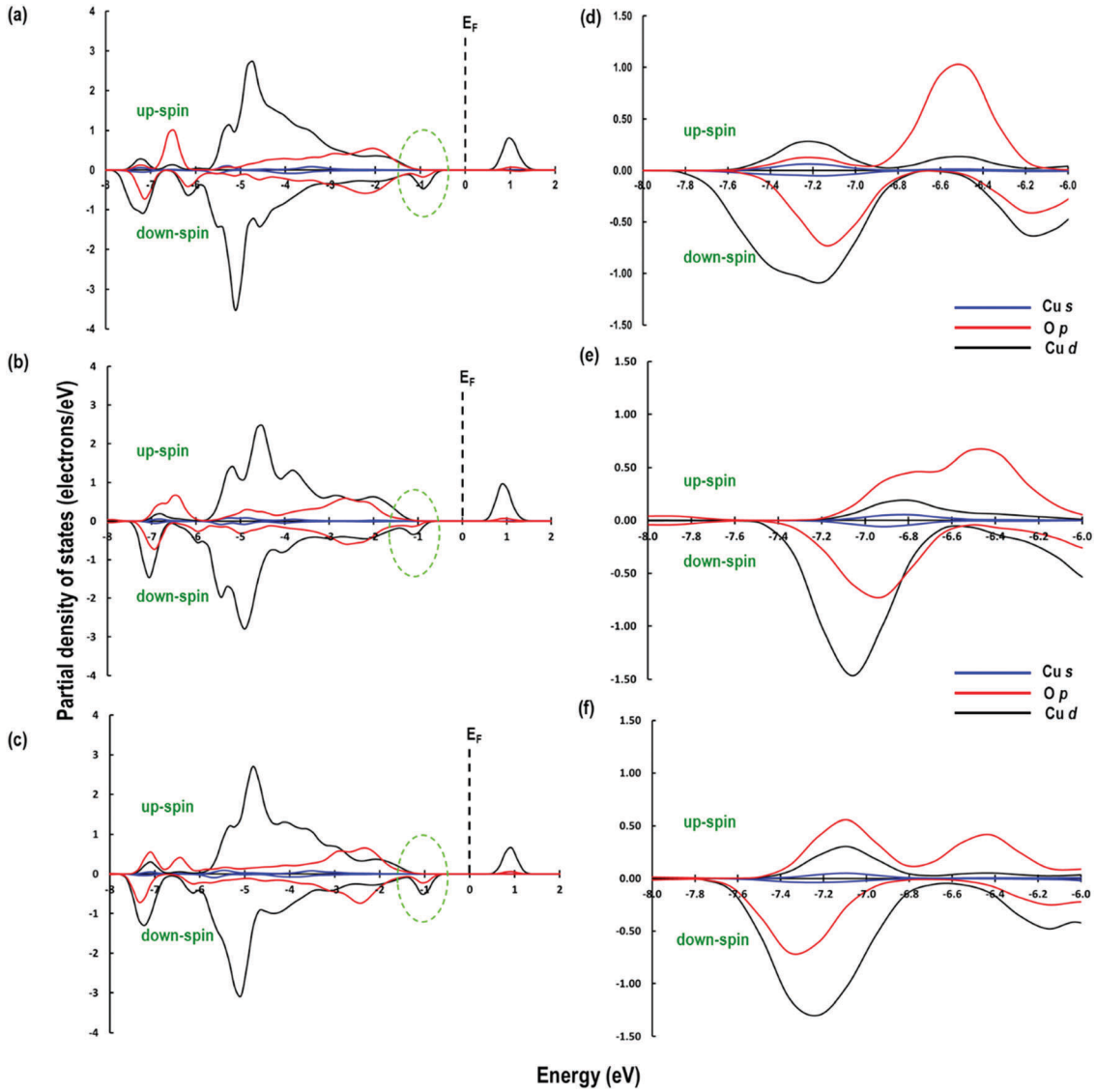

Fig. 13 Partial density of states for $Cu(OH)_2$ system with (a) one, (b) five and (c) fifteen water molecules. Partial density of states for $Cu(OH)_2$ system with (d) one, (e) five and (f) fifteen water molecules in the −8 eV to −6 eV.

which may be due to the interaction of Cu d-orbitals with the lone-pair O p-orbitals of the fifth O-atom coordinating to the Cu atom. This study show that a critical concentration of water molecules is required for obtaining a coordination number higher than four in the $Cu(OH)_2$–CeO_2 system and we conclude that the hydroxylated and solvated Cu^{2+} ion can explain the experimentally observed Cu–O coordination and estimated distances. We conclude that the model with five water molecules best rationalizes the experimental data and is consistent with the fact that the EXAFS data were measured on catalysts exposed to the atmosphere, probably having adsorbed water on the surface.

4. Summary and conclusions

The geometrical and adsorption properties of Cu species on the $CeO_2(110)$ surface are complex. An analysis of the PDOS shows that these unique properties are due to the contribution of low-lying Cu p-orbital and O s-orbital signatures. On the most stable structure clear charge transfer between Cu and the $CeO_2(110)$ surface is seen. Combined XANES and EXAFS studies with reference to Cu^0, Cu(I)oxide and Cu(II)oxide show the presence of Cu(II)O with Cu in +2 state. Based on the experimental findings, we then studied the local electronic properties of Cu(II) on the surface and in the bulk of $CeO_2(110)$ by substitution of a surface Ce–atom and creating an oxygen vacancy. The results show Cu–O bonds are close to the experimental values and the spin density of electrons highly localized around the Cu and O-atoms show strong bonding due to the hybridization between the Cu d and O p-orbital. To investigate further the experimentally observed O-atom environment around Cu(II) atom, we studied the interaction of $(CuO)_{n(=1,2\&4)}$ clusters on $CeO_2(110)$, which shows that, based on the Cu–O environment, the geometrical properties of these clusters may vary. We also conclude that the presence of

$(CuO)_n$ clusters leads to relatively higher localization of charges on the surface exposed to the $(CuO)_n$ clusters. Finally, studies on the $Cu(OH)_2/CeO_2(110)$ systems in the absence and presence of increasing concentrations of water molecules was carried out. From these calculations we conclude that in the presence of a critical concentration of water molecules, Cu is more stable with a coordination number of five with a square pyramidal geometry, which agrees well with our experimental findings, while in all other cases it has a coordination number of 4. We also conclude that Cu(II) facilitates water adsorption on $CeO_2(110)$ surface. Our study further shows that H transfer from water to $Cu(OH)_2/CeO_2(110)$ can take place. Analysis of the electron density difference shows a clear redistribution of charges on the $CeO_2(110)$ surface which varies with the concentration of water molecules used in the model. The calculated Cu–O bond distances are in close agreement with the experimentally observed values.

Conflicts of interest

There are no conflicts to declare.

Acknowledgements

We thank Dr Ricardo Grau-Crespo for his helpful discussions during the initial phase of this work. We thank Prof. Stefania Albonetti and Dr Alice Lolli for the synthesis of materials. We acknowledge Diamond Light Source for beamtime through awards SP10306 and SP15151, and thank the beamline scientists Dr Diego Gianolio and Dr Giannantonio Cibin. The UK Catalysis is thanked for resources and support provided *via* our membership of the UK Catalysis Hub consortium and funded by EPSRC (grants EP/K014706/1, EP/K014668/1, EP/K014854/1, EP/K014714/1, EP/M013219/1). *Via* our membership of the UK's HEC Materials Chemistry Consortium, which is funded by EPSRC (EP/L000202), this work used the ARCHER UK National Supercomputing Service (http://www.archer.ac.uk). We also thank HPCWales for computer time.

References

1 P. Bera, P. R. Sarode, M. S. Hegde, S. Emura, R. Kumashiro and N. P. Lalla, *Chem. Mater.*, 2002, **14**, 2120–2128.
2 D. H. Kim and J. E. Cha, *Catal. Lett.*, 2003, **86**, 107–112.
3 E. L. Wilson, C. L. Pang, G. Cabailh, Q. Chen, J. A. Purton, C. R. A. Catlow, W. A. Brown, N. H. De Leeuw and G. Thornton, *J. Phys. Chem. C*, 2008, **112**, 10918–10922.
4 J. Z. A. I. Liechtenstein and V. I. Anisimov, *Phys. Rev. B: Condens. Matter Mater. Phys.*, 1995, **52**, 5467–5471.
5 S. L. Dudarev, S. Y. Savrasov, C. J. Humphreys and A. P. Sutton, *Phys. Rev. B: Condens. Matter Mater. Phys.*, 1998, **57**, 1505–1509.
6 M. M. Branda, N. C. Hernández, J. F. Sanz and F. Illas, *J. Phys. Chem. C*, 2010, **114**, 1934–1941.
7 M. M. Branda, N. J. Castellani, R. Grau-Crespo, N. H. De Leeuw, N. C. Hernandez, J. F. Sanz, K. M. Neyman and F. Illas, *J. Chem. Phys.*, 2009, **131**, 094702.
8 L. Szabová, M. F. Camellone, M. Huang, V. Matoln and S. Fabris, *J. Chem. Phys.*, 2010, **133**, 234705.
9 L. Cui, Y. Tang, H. Zhang, L. G. Hector, C. Ouyang, S. Shi, H. Li and L. Chen, *Phys. Chem. Chem. Phys.*, 2012, **14**, 1923.
10 Y. Tang, H. Zhang, L. Cui, C. Ouyang, S. Shi, W. Tang, H. Li and L. Chen, *J. Power Sources*, 2012, **197**, 28–37.
11 N. C. Hernández, R. Grau-Crespo, N. H. de Leeuw and J. F. Sanz, *Phys. Chem. Chem. Phys.*, 2009, **11**, 5246–5252.
12 P. R. L. Keating, D. O. Scanlon, B. J. Morgan, N. M. Galea and G. W. Watson, *J. Phys. Chem. C*, 2012, **116**, 2443–2452.
13 A. B. Kehoe, D. O. Scanlon and G. W. Watson, *Chem. Mater.*, 2011, **23**, 4464–4468.
14 Z. Cheng, B. J. Sherman and C. S. Lo, *J. Chem. Phys.*, 2013, **138**, 014702.
15 Y. Chen, H. Wang, R. Burch, C. Hardacre and P. Hu, *Faraday Discuss.*, 2011, **152**, 121.
16 M. Fronzi, S. Piccinin, B. Delley, E. Traversa and C. Stampfl, *Phys. Chem. Chem. Phys.*, 2009, **2**, 9188–9199.
17 Z. Han and Y. Gao, *Chem. – Eur. J.*, 2016, **22**, 2092–2099.
18 N. Z. Koocher, J. M. P. Martirez and A. M. Rappe, *J. Phys. Chem. Lett.*, 2014, **5**, 3408–3414.
19 J. Carrasco, D. López-duran, Z. Liu, T. Duchon, J. Evans, S. D. Senanayake, E. J. Crumlin, V. Matolín, J. A. Rodríguez and M. V. Ganduglia-pirovano, *Angew. Chem., Int. Ed.*, 2015, **54**, 3917–3921.
20 J. Paier, C. Penschke and J. Sauer, *Chem. Rev.*, 2013, **113**, 3949–3985.
21 G. Kresse and J. Hafner, *Phys. Rev. B: Condens. Matter Mater. Phys.*, 1993, **47**, 558–561.
22 G. Kresse and J. Hafner, *Phys. Rev. B: Condens. Matter Mater. Phys.*, 1994, **49**, 14251–14269.
23 G. Kresse and J. Furthmüller, *Phys. Rev. B: Condens. Matter Mater. Phys.*, 1996, **54**, 11169–11186.
24 M. Nolan, S. Grigoleit, D. C. Sayle, S. C. Parker and G. W. Watson, *Surf. Sci.*, 2005, **576**, 217–229.
25 P. E. Blöchl, *Phys. Rev. B: Condens. Matter Mater. Phys.*, 1994, **50**, 17953–17979.
26 J. P. Perdew, K. Burke and M. Ernzerhof, *Phys. Rev. Lett.*, 1996, **77**, 3865–3868.
27 B. J. Morgan, D. O. Scanlon and G. W. Watson, *e-J. Surf. Sci. Nanotechnol.*, 2009, **7**, 389–394.
28 H. Raebiger, S. Lany and A. Zunger, *Phys. Rev. B: Condens. Matter Mater. Phys.*, 2007, **76**, 45209.
29 W. Tang, E. Sanville and G. Henkelman, *J. Phys.: Condens. Matter*, 2009, **21**, 84204.
30 G. Makov and M. Payne, *Phys. Rev. B: Condens. Matter Mater. Phys.*, 1995, **51**, 4014–4022.
31 J. Neugebauer and M. Scheffler, *Phys. Rev. B: Condens. Matter Mater. Phys.*, 1992, **46**, 16067–16080.
32 K. Momma and F. Izumi, *J. Appl. Crystallogr.*, 2011, **44**, 1272–1276.

33 K. Momma and F. Izumi, *J. Appl. Crystallogr.*, 2008, **41**, 653–658.
34 S. Scirè, P. M. Riccobene and C. Crisafulli, *Appl. Catal., B*, 2010, **101**, 109–117.
35 M. Newville, *J. Synchrotron Radiat.*, 2001, **8**, 322–324.
36 B. Ravel and M. Newville, *J. Synchrotron Radiat.*, 2005, **12**, 537–541.
37 J. Rothe, J. Hormes, H. Bonnemann, W. Brijoux and K. Siepen, *J. Am. Chem. Soc.*, 1998, **120**, 6019–6023.
38 Y. Chen, H. Wang, J. Li and J. V. Lockard, *J. Mater. Chem. A*, 2015, **3**, 4945–4953.
39 A. Gaur, W. Klysubun, B. Soni, B. D. Shrivastava, J. Prasad and K. Srivastava, *J. Mol. Struct.*, 2016, **1121**, 119–127.